

Testing general relativity's no-hair theorem with x-ray observations of black holes

Janie K. Hoormann,^{*} Banafsheh Beheshtipour, and Henric Krawczynski

*Physics Department and McDonnell Center for the Space Sciences, Washington University in St. Louis,
One Brookings Drive, CB 1105, St. Louis, Missouri 63130, USA*

(Received 28 October 2015; published 8 February 2016)

Despite its success in the weak gravity regime, general relativity (GR) has yet to be verified in the regime of strong gravity. In this paper, we present the results of detailed ray-tracing simulations aiming at clarifying if the combined information from x-ray spectroscopy, timing, and polarization observations of stellar mass and supermassive black holes can be used to test GR's no-hair theorem. The latter states that stationary astrophysical black holes are described by the Kerr family of metrics, with the black hole mass and spin being the only free parameters. We use four "non-Kerr metrics," some phenomenological in nature and others motivated by alternative theories of gravity, and study the observational signatures of deviations from the Kerr metric. Particular attention is given to the case when all the metrics are set to give the same innermost stable circular orbit in quasi-Boyer-Lindquist coordinates. We give a detailed discussion of similarities and differences of the observational signatures predicted for black holes in the Kerr metric and the non-Kerr metrics. We emphasize that even though some regions of the parameter space are nearly degenerate even when combining the information from all observational channels, x-ray observations of very rapidly spinning black holes can be used to exclude large regions of the parameter space of the alternative metrics. Although it proves difficult to distinguish between the Kerr and non-Kerr metrics for some portions of the parameter space, the observations of very rapidly spinning black holes like Cyg X-1 can be used to rule out large regions for several black hole metrics.

DOI: [10.1103/PhysRevD.93.044020](https://doi.org/10.1103/PhysRevD.93.044020)

I. INTRODUCTION

In the early 1900s, Albert Einstein proposed his now famous theory of general relativity. Since its introduction, general relativity (GR) has been tested extensively in our Solar System. GR has passed all tests with remarkable accuracy, including but not limited to the perihelion shift of Mercury, the deflection of light passing near the Sun, and the Shapiro time delay. These tests were extended beyond the Solar System with the discovery of the Hulse-Taylor binary pulsar where the decay rate of the orbital period was found to be consistent with the expected decay due to the loss of energy via gravitational waves (see [1] for a review of the subject). However, despite all of these successes, GR has yet to be verified in the strong gravity regime. The most extreme gravitational fields are found near black holes (BHs), and tests of GR near BHs have received considerable attention (see [2] and references therein). Much of this work makes use of the no-hair theorem of GR, which states that the only stationary axially symmetric solutions of the Einstein equations are given by the Kerr-Newman family of metrics. In the case of astrophysical BHs with negligible electrical charge, the Kerr solutions are parametrized by the BH's geometric mass, M , and spin, a . The tests of this theorem include using stars orbiting Sagittarius A*, the supermassive BH in the center of the Milky Way

galaxy, to measure its angular momentum and quadrupole moment [3]. Gravitational wave observations of merging black holes have the potential to test strong-field GR not only in the stationary but also in the dynamic regime [4]. The work presented in this paper makes use of several recently proposed metrics that contain additional terms which violate the no-hair theorem, including those of [5–8]. These metrics are used to quantify the degree to which spectroscopic, polarimetric, and timing x-ray observations can constrain deviations from the Kerr metric.

The spectral x-ray emission from stellar mass BHs can be characterized by a thermal continuum emitted from the accretion disk along with a power-law component originating from hotter—yet mostly thermal—plasma, commonly referred to as the corona (e.g., [9]). The power-law emission is modeled using the equation $N(E) \propto E^{-\Gamma}$ where Γ is the photon index [10]. This emission can either travel directly to the observer or return to the accretion disk and lead to scattered and/or reprocessed emission. The reflection component contains the Fe-K α line at 6.4 keV and the Compton hump at energies greater than 20 keV. The prominent Fe-K α line comes from the reprocessing of photons in the inner accretion disk and receives its characteristic broadened profile due to gravitational redshift, Doppler effects, and relativistic beaming. This profile can then be fit to determine the BH's spin [11–13]. The thermal emission, modeled using the prescription developed by [14] for a geometrically thin, optically thick disk,

^{*}jhoormann@wustl.edu

can also be used to deduce the spin of stellar mass black holes because it allows one to determine the radius of the innermost stable circular orbit (ISCO) which is a monotonic function of its spin [15,16]. In the case of supermassive black holes, the thermal disk emission falls into the optical/UV bands. As many different emission components contribute to the observed emission in these bands, fitting the Fe-K α line is the only way to determine the spin of these systems.

Polarimetric observations with photoelectric effect polarimeters like the ones used on the IXPE, PRAXyS, and XIPE missions currently studied by NASA (IXPE [17] and PRAXyS [18]) and ESA (XIPE [19]) or with scattering polarimeters such as PolSTAR [20–22] provide a new way to study the inner structure of accretion flows. Polarimeters can provide geometrical information even though the inner accretion flow of most black holes is too small to be imaged with the current or even next-generation telescopes (the only exception being the supermassive black holes Sgr A* and M 87 which might be imaged with the Event Horizon Telescope [23]). In the case of stellar mass black holes, the thermal x-ray emission is expected to exhibit linear polarization with the polarization fraction being a function of the inclination of the inner accretion disk [24,25]. The polarization of the Comptonized emission from the corona depends on the scattering processes in the corona itself and off the accretion disk. Several corona geometries have been studied, including the lamp-post model where photons are emitted from a point source directly above the black hole itself [26]. Other corona models assume a wedge or spherical corona geometry surrounding the accretion disk (e.g., [27] and references therein).

In the past several years x-ray reverberation has come into its own as a powerful tool to study accreting black holes. Corona emission scattering off the accretion disk reaches the observer with a time delay relative to the direct corona emission. The energy dependence of the time delays can be used to infer details about the structure of the inner accretion flow. For a sample of active galactic nuclei (AGN), Fe-K α vs continuum lags have been established along with Compton hump vs continuum lags (see [28,29] for a review of the subject). These lags can be fit with numerical models to deduce system parameters such as the inclination and lamp-post height in NGC 4151 [30] and an extended corona geometry in 1H0707-495 [31].

Several authors have used the alternative BH metrics to find observational signatures of non-GR effects. The following types of observations have been studied: (i) fitting of the thermal x-ray emission from stellar mass black holes [32–34]; (ii) fitting of the Fe-K α line emission from stellar mass and supermassive black holes [35–38]; (iii) spectropolarimetric observations of stellar mass black holes [39,40]; (iv) observations of quasiperiodic oscillations (QPOs) [41–43]; (v) x-ray reverberation observations [44]; and (vi) observations of the radiatively inefficient

accretion flow around Sgr A* [45]. The studies showed that it is very difficult to observationally distinguish between the Kerr spacetime and the non-Kerr BH spacetimes as long as the BH spin and the parameter describing the deviation from the Kerr spacetime are free parameters that both need to be derived from the observations.

Several approaches have been discussed to break the degeneracy between the BH spin and deviation parameter (s). In [33,46], for example, it is proposed that the BH spin can be measured independently from the accretion disk properties based on measuring the jet power, although this method faces several difficulties in practice [47]. Furthermore, the observed results depend on the physics of the accretion disk, the radiation transport around the black hole, the physics of launching and accelerating the jet, and the physics of converting the mechanical and electromagnetic jet energy into observable electromagnetic jet emission.

This paper follows up on the work of [39]. The thermal emission from a geometrically thin, optically thick accretion disk is modeled self-consistently for the Kerr metric and the alternative metrics, and observational signatures are derived with the help of a ray-tracing code that tracks photons from their origin to the observer, enabling the modeling of repeated scatterings of the photons off the accretion disk. This paper adds to the previous work by (i) covering the Kerr metric, the metric of Johannsen and Psaltis [5] and three additional metrics, (ii) by modeling not only the thermal disk emission but also the emission from a lamp-post corona and the reprocessing of the coronal emission by the accretion disk, and (iii) by considering many observational channels. We analyze the multitemperature continuum emission from the accretion disk, the energy spectra of the reflected emission (including the Fe-K α line and the Compton hump), the orbital periods of matter orbiting the black hole close to the ISCO, the time lags between the Fe-K α emission and the direct corona emission, and the size and shape of the black hole shadows.

The rest of the paper is organized as follows. Section II begins with a summary of the alternative spacetimes used in this paper and goes on to discuss the model for both the thermal and coronal emission. In Sec. III we compare the observational signatures of the Kerr and non-Kerr metrics finding that the observational differences are rather small given the uncertainties about the properties of astrophysical accretion disks. We summarize the results in Sec. IV and emphasize that even though the Kerr and non-Kerr metrics can produce similar observational signatures for some regions of the respective parameter spaces, we can use x-ray observations of black holes from the literature to rule out large regions of the parameter space of the non-Kerr metrics.

Throughout this paper we assume $c = \hbar = G = 1$; all distances are given in units of the gravitational radius, $r_g = GM/c^2$.

II. METHODOLOGY

A. Alternative metrics

As a way to test the no-hair theorem of general relativity, several non-Kerr metrics have been introduced which contain additional parameters apart from the BH's mass and spin. In this paper we employ the use of four non-GR metrics including two phenomenological metrics [5,6] and two which are solutions to alternative theories of gravity [7,8]. All metrics are variations of the Kerr metric in (quasi-)Boyer-Lindquist coordinates $x^\mu = (ct, r, \theta, \phi)$.

The phenomenological metric of Johannsen and Psaltis [5] (JP) reads

$$\begin{aligned}
 ds^2 = & -[1 + h(r, \theta)] \left(1 - \frac{2Mr}{\Sigma} \right) dt^2 - \frac{4aMr \sin^2 \theta}{\Sigma} \\
 & \times [1 + h(r, \theta)] dt d\phi + \frac{\Sigma [1 + h(r, \theta)]}{\Delta + a^2 \sin^2 \theta h(r, \theta)} dr^2 \\
 & + \Sigma d\theta^2 + \left[\sin^2 \theta \left(r^2 + a^2 + \frac{2a^2 Mr \sin^2 \theta}{\Sigma} \right) \right. \\
 & \left. + h(r, \theta) \frac{a^2 (\Sigma + 2Mr) \sin^4 \theta}{\Sigma} \right] d\phi^2 \quad (1)
 \end{aligned}$$

with

$$\Sigma \equiv r^2 + a^2 \cos^2 \theta \quad (2)$$

$$\Delta \equiv r^2 - 2Mr + a^2. \quad (3)$$

The metric was derived by modifying the temporal and radial components of the Schwarzschild line element by a term $h(r, \theta)$. The metric does not exhibit any pathologies outside the event horizon and can be used for slowly and rapidly spinning black holes. Asymptotic flatness constrains the leading terms of the expansion of h in powers of r and the lowest order correction reads

$$h(r, \theta) = \epsilon_3 \frac{M^3 r}{\Sigma^2}. \quad (4)$$

In the limit as $\epsilon_3 \rightarrow 0$ this metric reduces to the Kerr solution in Boyer-Lindquist coordinates.

Glampedakis and Babak [6] (GB) introduced a metric for slowly spinning black holes ($a \lesssim 0.4$). This quasi-Kerr metric in Boyer-Lindquist coordinates is

$$g_{ab} = g_{ab}^K + \epsilon h_{ab} \quad (5)$$

where g_{ab}^K is the Kerr metric and h_{ab} is given by

$$\begin{aligned}
 h^{tt} &= \left(1 - \frac{2M}{r} \right)^{-1} [(1 - 3\cos^2 \theta) \mathcal{F}_1(r)] \\
 h^{rr} &= \left(1 - \frac{2M}{r} \right) [(1 - 3\cos^2 \theta) \mathcal{F}_1(r)] \\
 h^{\theta\theta} &= -\frac{1}{r^2} [(1 - 3\cos^2 \theta) \mathcal{F}_2(r)] \\
 h^{\phi\phi} &= -\frac{1}{r^2 \sin^2 \theta} [(1 - 3\cos^2 \theta) \mathcal{F}_2(r)] \\
 h^{t\phi} &= 0 \quad (6)
 \end{aligned}$$

where $\mathcal{F}_1(r)$ and $\mathcal{F}_2(r)$ are defined in Appendix A in [6]. It is clear to see that Eq. (5) reduces to the Kerr metric when $\epsilon \rightarrow 0$. The details of the JP and GB spacetimes are described in [48].

Another solution is presented by Aliev and Gümrükçüoğlu [7] describing an axisymmetric, stationary metric for a rapidly rotating black hole which is on a 3-brane in the Randall-Sundrum braneworld. The metric turns out to be identical to GR's Kerr-Newman metric of an electrically charged spinning black hole, the only difference that β is not the electrical charge but a "tidal charge." The metric (referred to as the KN metric in the following) is given by

$$\begin{aligned}
 ds^2 = & - \left(1 - \frac{2Mr - \beta}{\Sigma} \right) dt^2 - \frac{2a(2Mr - \beta)}{\Sigma} \\
 & \times \sin^2 \theta dt d\phi + \frac{\Sigma}{\Delta} dr^2 + \Sigma d\theta^2 \\
 & + \left(r^2 + a^2 + \frac{2Mr - \beta}{\Sigma} a^2 \sin^2 \theta \right) \sin^2 \theta d\phi^2 \quad (7)
 \end{aligned}$$

with Σ being the same as Eq. (2) and with $\Delta = r^2 + a^2 - 2Mr + \beta$.

Pani *et al.* [8] (PMCC) give a family of solutions for slowly rotating BHs derived augmenting the Einstein-Hilbert action by quadratic and algebraic curvature invariants coupling to a single scalar field. The action is given by the expression

$$\begin{aligned}
 S = & \frac{1}{16\pi} \int \sqrt{-g} d^4x [R - 2\nabla_a \phi \nabla^a \phi - V(\phi) + f_1(\phi) R^2 \\
 & + f_2(\phi) R_{ab} R^{ab} + f_3(\phi) R_{abcd} R^{abcd} \\
 & + f_4(\phi) R_{abcd} {}^* R^{abcd}] + S_{mat}[\gamma(\phi) g_{\nu\mu}, \Psi_{mat}] \quad (8)
 \end{aligned}$$

where

$$f_i(\phi) = \eta_i + \alpha_i \phi + \mathcal{O}(\phi^2) \quad (9)$$

for $i = 1 - 4$, where S_{mat} is the matter action containing a generic nonminimal coupling, and $V(\phi)$ is the scalar self-potential. When $\alpha_3 = 0$ the metric reduces to the one for Chern-Simons gravity and when $\alpha_4 = 0$ it becomes the Gauss-Bonnet solution.

B. Thermal accretion disk emission and photon propagation

The code models the emission of photons and their propagation self-consistently for the Kerr and non-Kerr metrics [39]. The radial emission profile of the geometrically thin, optically thick accretion disk is calculated based on the general solution of Novikov and Thorne [14], the relativistic extension of the Shakura-Sunyaev equations [49]. Writing the considered Kerr or non-Kerr metric in the form

$$ds^2 = -e^{2\nu} dt^2 + e^{2\psi} (d\phi - \omega dt)^2 + e^{2\mu} dr^2 + dz^2, \quad (10)$$

the conservation of rest mass, angular momentum, and energy give the following disk brightness $F(r)$ in the rest frame of the emitting plasma [50]:

$$F(r) = \frac{\dot{M}_0}{4\pi} e^{-(\nu+\psi+\mu)} f(r) \quad (11)$$

with

$$f(r) \equiv \frac{-p^t_{;r}}{p_\phi} \int_{r_{\text{ISCO}}}^r \frac{p_{\phi;r}}{p^t} dr. \quad (12)$$

Here, \dot{M}_0 is the time averaged rate of accretion. The solution assumes a vanishing torque at the ISCO. We calculate the r_{ISCO} by finding the location where the energy is a minimum by solving the equation $\frac{dE}{dr} = 0$ for planar, circular orbits.

We model photons emitted between r_{ISCO} and $100r_g$ that are tracked until they either fall into a black hole or reach a coordinate stationary observer at $r = 10,000r_g$. The photon trajectories are calculated by integrating the geodesic equations:

$$\frac{d^2 x^\mu}{d\lambda'^2} = -\Gamma^\mu_{\sigma\nu} \frac{dx^\sigma}{d\lambda'} \frac{dx^\nu}{d\lambda'} \quad (13)$$

with a fourth order Runge-Kutta method. The $\Gamma^\mu_{\sigma\nu}$'s are the Christoffel symbols and λ' is the affine parameter. Tracking photons forward in time makes it possible to model trajectories with multiple scattering events and/or with the absorption and reemission of photons in the accretion disk and/or in the corona. The initial polarization and the change in polarization upon scattering are calculated with the help of Chandrasekhar's results for optically thick atmospheres [51]. The polarization vector, \mathbf{f} , is parallel transported according to the following equation:

$$\frac{df^\mu}{d\lambda'} = -\Gamma^\mu_{\sigma\nu} f^\sigma \frac{dx^\nu}{d\lambda'}. \quad (14)$$

A more detailed description of the code can be found in [39].

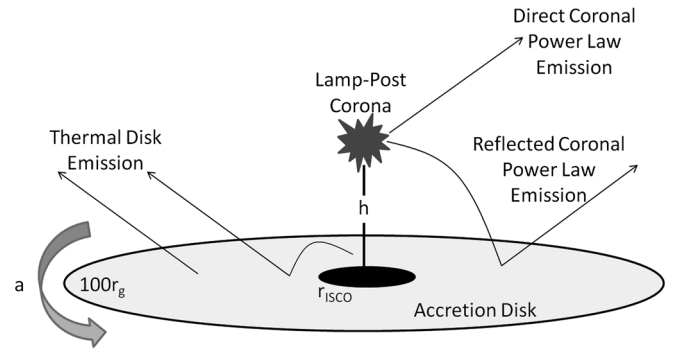


FIG. 1. Diagram showing the thermal and coronal lamp-post emission surrounding a black hole.

C. Lamp-post corona model

We utilize the commonly used lamp-post model (e.g., [52,53]) to simulate the coronal power-law emission. Unpolarized 1–100 keV photons are emitted from a point

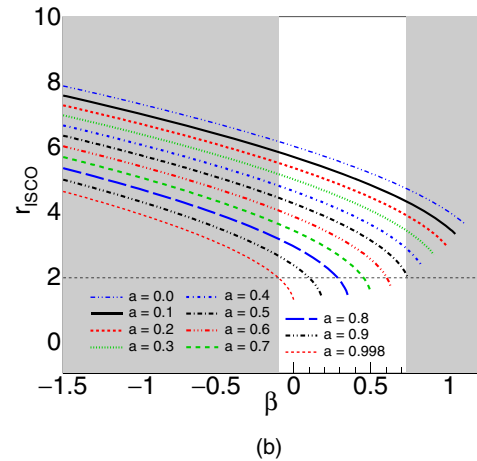
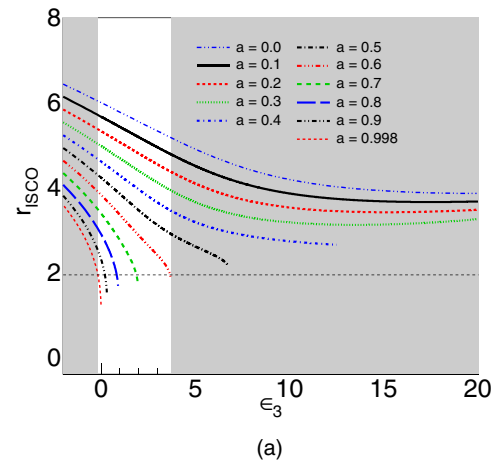


FIG. 2. r_{ISCO} as a function of deviation parameter for the JP metric (a) and the KN metric (b) with different spins illustrating the degeneracies within the metrics. The regions shaded grey indicate the portion of the parameter space excluded by observations of Cyg X-1 where the observed r_{ISCO} [56] is represented by the horizontal dashed black line.

TABLE I. List of metric parameters used in the simulations.

Metric	Spin	Deviation	r_{ISCO}	\dot{M} (g/s)
Kerr	0.9	none	2.32	8.98×10^{17}
JP	0.5	$\epsilon_3 = 6.33$	2.32	7.51×10^{17}
KN	0.5	$\beta = 0.69$	2.32	9.86×10^{17}
Kerr	0.2	none	5.33	2.16×10^{18}
GB	0.25	$\epsilon = 0.12$	5.33	2.15×10^{18}
PMCC	0.29	$\alpha_3 = 0, \alpha_4 = 2.07$	5.33	2.11×10^{18}

source above the black hole. The height of the point source can be constrained based on fitting the Fe-K α vs continuum emission lag (e.g., [30]). Alternatively, the corona may be associated with a region of energy dissipation close to the base of a jet. The trajectory of the photons and their change in polarization upon scattering off the accretion disk are calculated as described above. Photons impinging on the accretion disk can either be absorbed, prompt the emission of a Fe-K α fluorescence photon, or Compton scatter. A diagram of the various types of emission modeled can be seen in Fig. 1. The results of [54] were used to determine the probability of the creation of the Fe-K α photons and Compton reflections. The results can then be analyzed to examine the time lag between the direct power-law emission and the Fe-K α emission from 2–10 keV following the methodology described in [30]. We analyze the Fourier

transform of the transfer function to infer the time lag as a function of Fourier frequency.

III. RESULTS

Previous analyses have shown that the Kerr and non-Kerr metrics give similar spectral and spectropolarimetric signatures if the parameters are chosen to give the same r_{ISCO} (e.g., [35,37,39,43,44,55]). Figure 2 shows r_{ISCO} as a function of the BH spin a and the parameter characterizing the deviation from the Kerr metric for the JP and KN metrics. We see that for all JP and KN metrics, we can always find one and only one Kerr metric with the same r_{ISCO} . The mapping is not unambiguous the other way around: the JP and KN metrics can give one r_{ISCO} for several different combinations of the BH spin a and the deviation parameter.

In the following we focus on comparing “degenerate” models which give the same r_{ISCO} . We consider a slowly spinning Kerr black hole ($a = 0.2$, $r_{\text{ISCO}} = 5.33r_g$) and a rapidly spinning Kerr black hole ($a = 0.9$, $r_{\text{ISCO}} = 2.32r_g$) and JP and KN models giving the same r_{ISCO} (see Table I). In the following we show the Kerr, GB, and PMCC results for the low-spin case, and the Kerr, KN, and JP results for the high-spin case. We adjusted the accretion rates to give the same accretion luminosity (extracted gravitational energy per unit observer time) for all considered metrics.

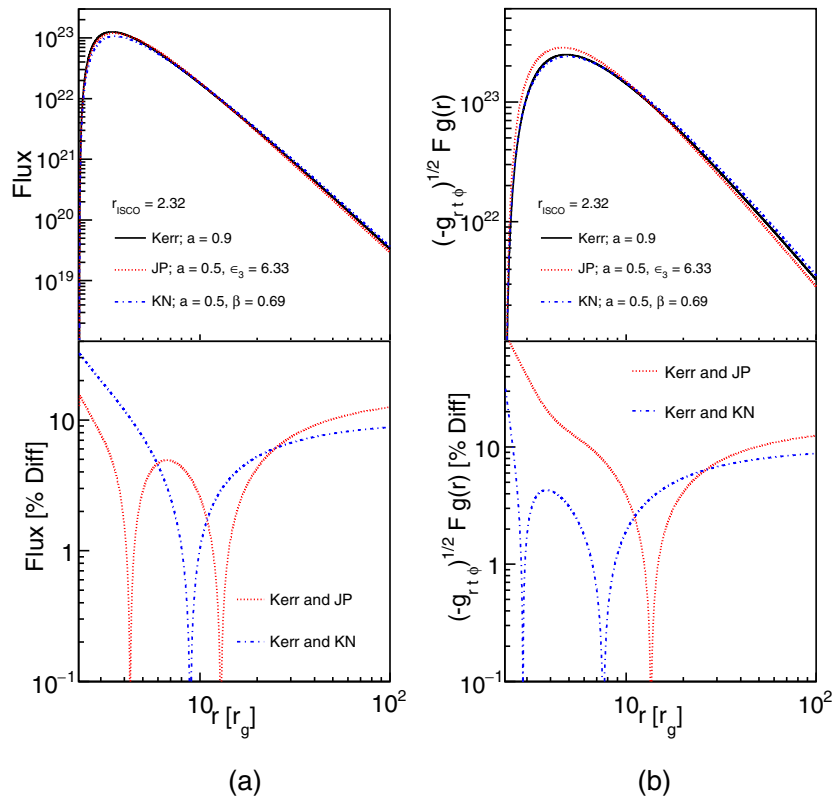


FIG. 3. Radial flux [Eq. (11)] (a) and power (b) for the JP, KN, and Kerr metrics, which all give $r_{\text{ISCO}} = 2.32r_g$. The bottom panels show the comparison of the alternative metrics to the Kerr metric.

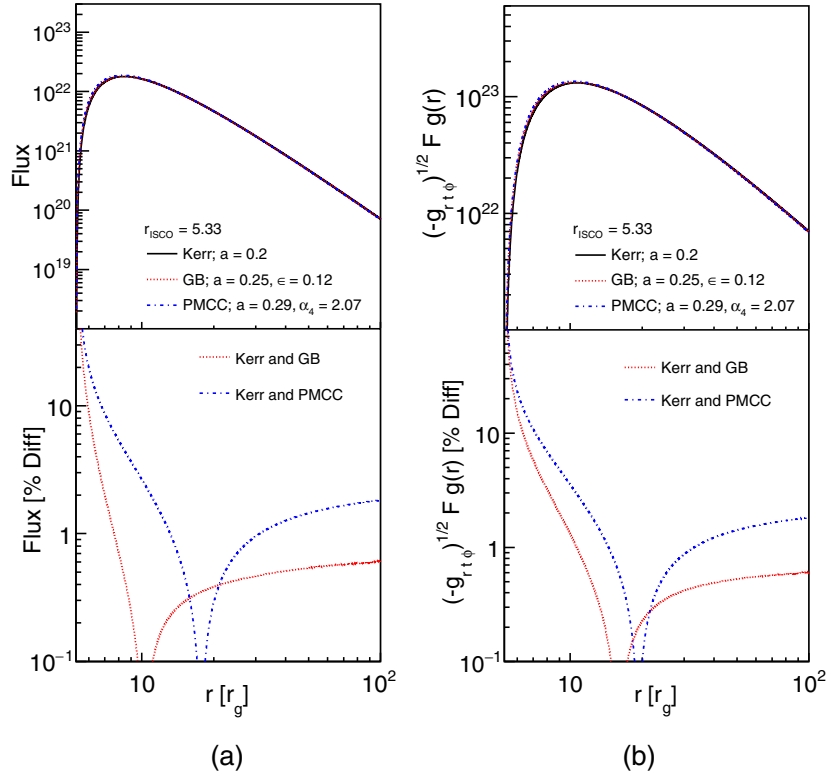


FIG. 4. Radial flux [Eq. (11)] (a) and power (b) for the GB, PMCC, and Kerr metrics, which all give $r_{\text{ISCO}} = 5.33r_g$. The bottom panels show the comparison of the alternative metrics to the Kerr metric.

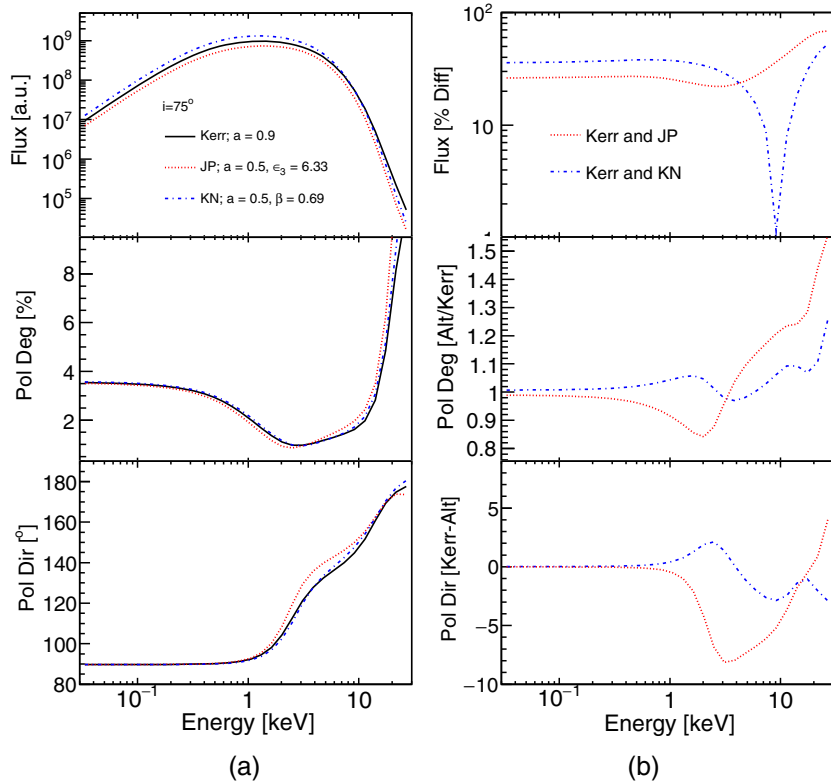


FIG. 5. Flux (top panel), polarization fraction (middle panel), and polarization degree (bottom panel) of the thermal disk emission for the JP, KN, and Kerr metrics (a) and corresponding comparisons of the alternative metrics with respect to the Kerr metric (b).

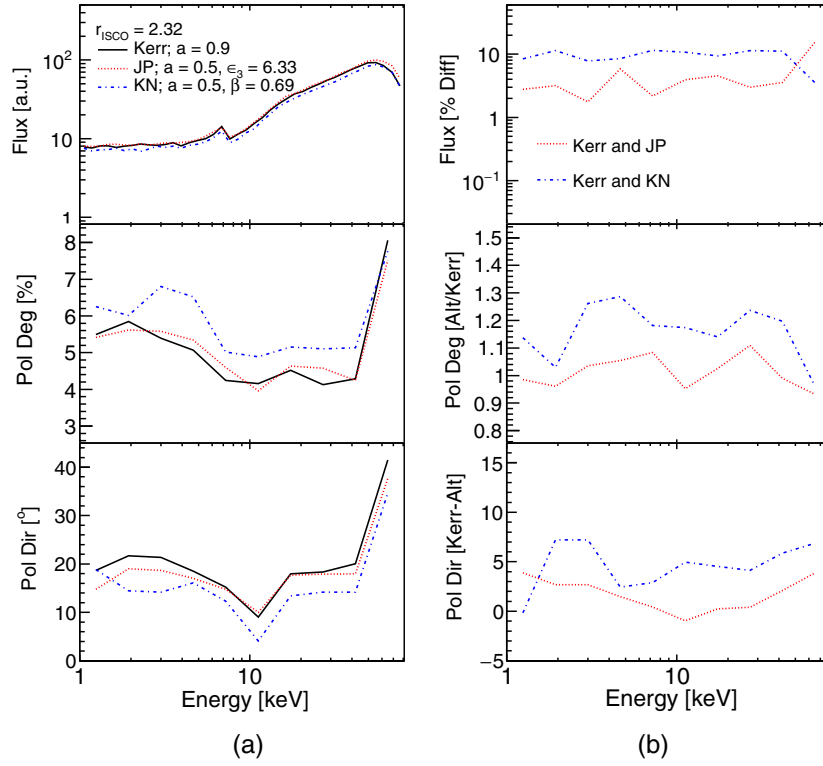


FIG. 6. Flux (top panel), polarization fraction (middle panel), and polarization degree (bottom panel) for the reflected spectrum showing the Fe- $K\alpha$ line of an AGN with $h = 3r_g$ for the JP, KN, and Kerr metrics (a) and corresponding comparisons of the alternative metrics with respect to the Kerr metric (b).

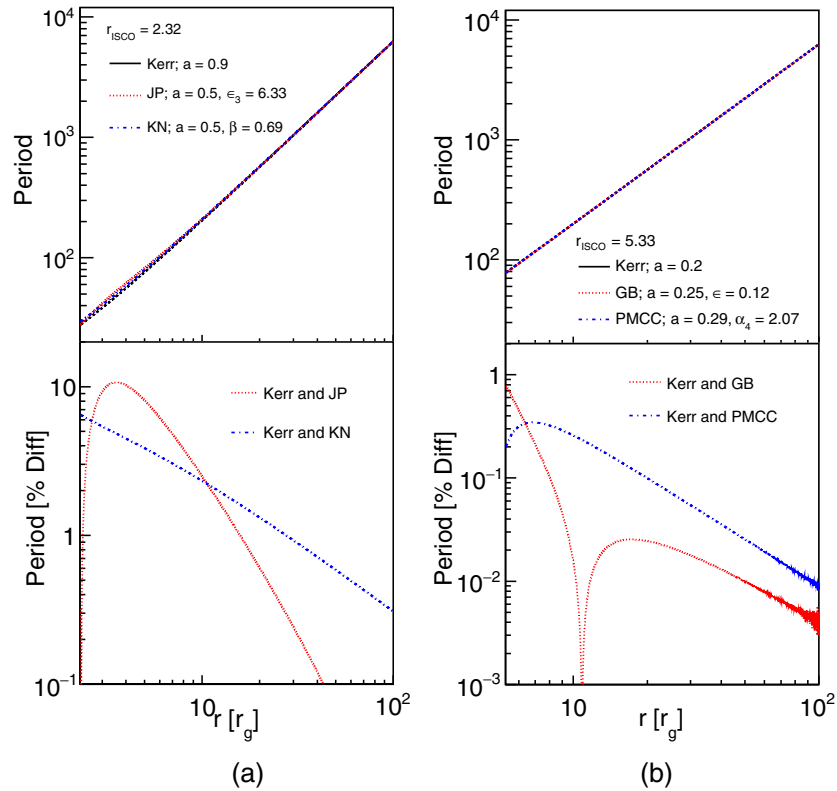


FIG. 7. Orbital periods (top panels) for the metrics and the percent difference (bottom panels) for the JP and KN metrics compared to the Kerr metric (a) and the GB and PMCC metrics (b).

This is done by normalizing the accretion rate by the efficiency, which is not corrected for the fraction of photons escaping to infinity.

The left panels of Figs. 3 and 4 compare the fluxes $F(r)$ emitted in the plasma frame for the different metrics. For the rapidly spinning black holes [Fig. 3(a)], the fractional differences in $F(r)$ are typically a few percent. The difference is larger for the innermost part of the accretion flow with the Kerr $F(r)$ exceeding the values of the non-Kerr metrics by up to 30%.

The right panels of the figures show the power P emitted per unit Boyer-Lindquist time and per Boyer-Lindquist radial interval dr :

$$\frac{dP}{dr}(r) = \sqrt{-g_{t\phi}} F(r) g_{\text{em}}^{\text{obs}} \quad (15)$$

The factor $\sqrt{-g_{t\phi}}$ is the $t-r-\phi$ dependent part of the metric and is used to transform the *number* of emitted photons per plasma frame $d\hat{t}$ and $d\hat{r}$ into that emitted per Boyer-Lindquist dt and dr [57]. The last factor corrects for the frequency change of the photons between their emission in the plasma rest frame and their detection by an observer at infinity. We estimate the effective redshift between emission and observation by assuming photons are emitted in the upper hemisphere with the dimensionless wave vector $\hat{k}^\mu = (1, 0, -1, 0)$ in the plasma frame. After transforming \hat{k} into the wave vector k in the Boyer-Lindquist frame we calculate the photon energy at infinity E_γ from the constant of motion associated with the time translation Killing vector $(1, 0, 0, 0)$:

$$E_\gamma = -k_t \quad (16)$$

and set $g_{\text{em}}^{\text{obs}} = E_\gamma$. The different metrics exhibit very similar dP/dr distributions with typical fractional differences of $< 10\%$. Again, the largest deviations are found near the ISCO. Overall, the different metrics lead to very similar $F(r)$ and dP/dr distributions because (i) we compare models with identical r_{ISCO} values (leading radial profiles with a similar r dependence), and (ii) we use fine-tuned accretion rates \dot{M} to compensate for the different accretion efficiencies where $\eta = 1 - E_{\text{ISCO}}$ (i.e., the different fractions of the rest mass energy that can be extracted when matter moves from infinity to r_{ISCO}). In the following we focus on the rapidly spinning BH simulations, as the observables depend more strongly on the assumed background spacetime than for slowly spinning BHs.

The analysis presented here focuses on specific choices for matching the Kerr metric with non-Kerr counterparts. This matching is not unique as the non-Kerr metrics give the same r_{ISCO} for a continuous family of different metrics. We simulated a few non-Kerr metrics giving the same r_{ISCO} , and found that the differences between these metrics and the Kerr metric are all comparable to the differences shown above.

Figure 5 shows the flux, polarization degree, and polarization direction of the thermal disk emission of a mass accreting stellar mass BH as shown for an observer at an inclination of 75° . We only show the results for the rapidly spinning Kerr, JP, and KN BHs. While there are some differences in these spectra the overall shapes are similar. At the highest energies, deep in the Wien tail of the multitemperature energy spectrum, the fluxes show more differences owing to the different orbital velocities and thus Doppler boost of the emission and different fractions of photons reaching the observer versus photons falling into the BHs. The different metrics also lead to very similar polarization fractions and polarization angles. However, in terms of the polarization properties the Kerr and KN metrics show almost identical results and the JP metric shows slightly different results. Overall, the main conclusion is that once we choose models with identical r_{ISCO} and correct for the different accretion efficiencies, the observational signatures depend only very weakly on the considered metric. Assuming that the background spacetime is described by the Kerr metric, the thermal energy

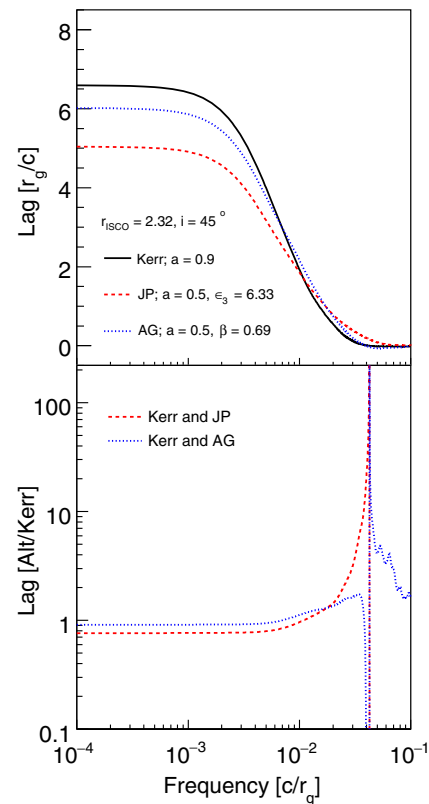


FIG. 8. Lag-frequency spectrum (top panel) of an AGN with $h = 3r_g$ for the JP, KN, and Kerr metrics along with the percent difference (bottom panel) of the KN and JP metrics when compared with the Kerr metric. A positive lag corresponds to the reflected emission lagging behind the direct emission where the direct emission is given in the 1 to 2 keV band and the reflected emission is in the 2–10 keV band.

spectrum and the polarization properties can be used to fit r_{ISCO} and the BH inclination i [24,25]. The results presented so far indicate that the fitted r_{ISCO} and i values will not depend strongly on the assumed background spacetime.

We now turn to the properties of the reflected corona emission from an AGN, assuming that the lamp-post corona emits unpolarized emission with a photon power-law index of $\Gamma = 1.7$ from a height $h = 3r_g$ above the black hole (Fig. 6). Again, the flux and polarization energy spectra are almost the same for all considered metrics. The KN metric shows slightly larger deviations from the Kerr metric than the JP metric.

Some accreting black holes exhibit QPOs, i.e., peaks in the Fourier transformed power spectra. The orbiting hot spot model [58–63] explains the high-frequency QPOs (HFQPOs) of accreting stellar mass black holes with a hot spot orbiting the black hole close to the ISCO. If we succeeded in confirming the model (e.g., through the observations of the phase resolved energy spectra and/or polarization properties [64]), one could use HFQPO observations to measure the orbital periods close to the ISCO. In the case of AGNs, tentative evidence for periodicity associated with the ISCO has been found for several objects. Examples include orbital periodicity on the time scale of a few days as seen in the blazar OJ 287 [65] and QPOs at frequencies of O(100 Hz) such as that seen for the

microquasar GRO J1655-40 [66]. Figure 7 shows that different metrics do predict different orbital periods which vary by up to $\sim 10\%$.

We investigated if other *timing properties* can be used to observationally distinguish between the different metrics by analyzing the observable time lags between the direct corona emission and the reflected emission assuming the lamp-post geometry. We use the standard x-ray reverberation analysis methods described by [29]. As expected, the 2–10 keV flux variations lag the 1 to 2 keV flux variations (Fig. 8). The JP metric leads to time lags up to 24% shorter than the Kerr and KN metrics at low frequencies. At frequencies between $0.01c/r_g$ and $0.1c/r_g$ phase wrapping begins to occur (when the lag changes sign and begins to oscillate around 0) leading to the larger differences seen in this range.

Although the considered metrics give the same r_{ISCO} in Boyer-Lindquist coordinates, the black hole shadow may have a different shape and/or size when viewed by an observer at infinity (see [67,68] for a related study). The results for the Kerr, JP, and KN metrics are shown in Fig. 9 for an inclination of $i = 75^\circ$. The shadow of the KN and JP metrics is $\sim 15\%$ smaller than that of the Kerr metric. Furthermore, the shapes differ slightly. Similarly, the shapes of the photon rings are shown in Fig. 10, which are calculated by following the procedures outlined in Sec. III of [69].

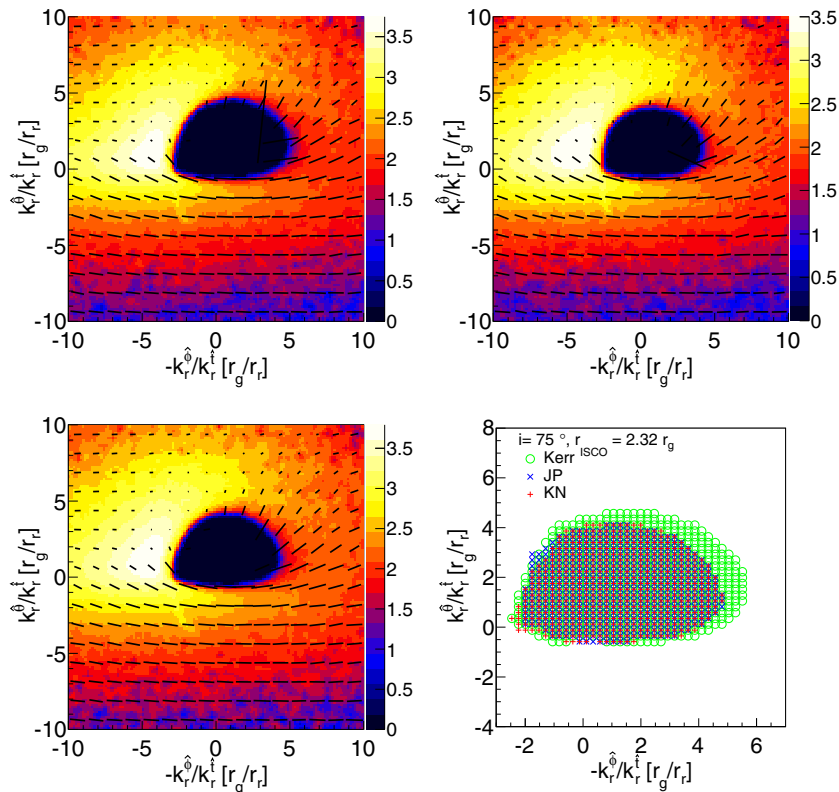


FIG. 9. Intensity-polarization maps of the three rapidly spinning metrics in Kerr (top left panel), JP (top right panel), KN (bottom left panel) for a black hole at a high inclination along with a comparison of their shadows (bottom right panel).

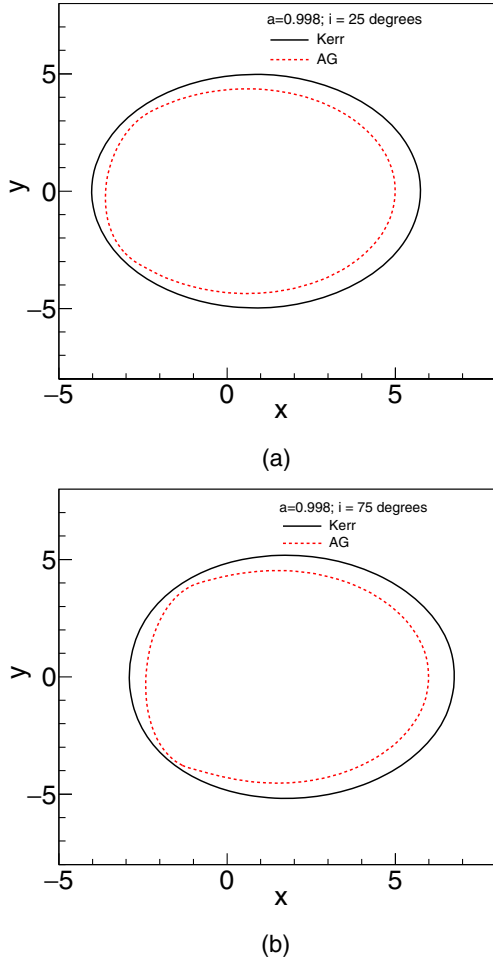


FIG. 10. Photon rings of the Kerr and KN metrics as seen by an observer at both $i = 25^\circ$ (a) and $i = 75^\circ$ (b).

IV. SUMMARY AND DISCUSSION

In this paper we studied the observational differences between accreting black holes in five different background spacetimes, including GR's Kerr spacetime, and four alternative spacetimes. We chose the parameters of the considered metrics so as to give identical innermost stable orbits in Boyer-Lindquist coordinates. The predicted observational differences are larger for rapidly spinning black holes. Overall the observational differences are very small if we adjust the accretion rate to correct for the metric-dependent accretion efficiency. The measurement of the predicted differences are very small—especially if one accounts for the astrophysical uncertainties, i.e., observational and theoretical uncertainties of the accretion disk properties. From an academic standpoint, it is interesting to compare the small differences of the predicted properties, e.g., the differences of the thermal energy spectra and the

BH shadow images. The thermal spectrum of the Kerr BH is slightly harder than that of the JP and KN black holes (for the same r_{ISCO}), and the Kerr BH shadow is slightly larger than that of the JP and KN BH shadows. Reducing the spin of the Kerr BH would make the spectral difference smaller, but would increase the mismatch between the apparent BH shadow diameters. Thus, in the absence of astrophysical uncertainties, the combined information from various observational channels could be used to distinguish between different metrics.

Although the analysis shows that the differences between the Kerr and non-Kerr metrics are rather subtle (especially in the presence of uncertainties of the structure of astrophysical accretion disks), we can use existing observations to constrain large parts of the parameter space of the non-Kerr metrics (see also [70]). As an example we use the recent observations of the accreting stellar mass black hole Cyg X-1 [56]. The observations give a 3σ upper limit of $r_{\text{ISCO}} < 1.94$. Inspecting Fig. 2 we see that the constraints on the ISCO can only be fulfilled for JP deviation parameters $\epsilon_3 \in [-0.15, 3.72]$ and KN deviation parameters $\beta \in [-0.01, 0.73]$, excluding all parameter values outside of these intervals. Our limits rest on the matching of Kerr to non-Kerr metrics via using identical r_{ISCO} values. Maximally rotating black holes, when $a = 0.998$ [71], provide the best opportunity to test GR because observations of these systems can, in principle, be used to exclude all deviations from GR down to a small interval around 0, limited only by the actual spin value, the statistics of the observations, and the astrophysical uncertainties. A follow-up analysis could use state-of-the-art modeling of the actual x-ray data with accretion disk and emission models in the Kerr and non-Kerr background spacetimes.

Further progress will be achieved by continuing to refine our understanding of BH accretion disks based on general relativistic magnetohydrodynamic and general relativistic radiation magnetohydrodynamic simulations (e.g., [72–74]) and matching simulated observations to x-ray spectroscopic, x-ray polarization, and x-ray reverberation observations.

The images of the BH shadow of Sgr A* with the Event Horizon Telescope can give additional constraints. Whereas the images of the BH shadow still depend on the astrophysics of the accretion disk, imaging of the photon ring would be free of such uncertainties. Of course, much better imaging would be required to do so.

ACKNOWLEDGMENTS

We would like to thank NASA (Grant No. NNX14A D19G) and the Washington University McDonnell Center for the Space Sciences for their financial support.

- [1] C. M. Will, *Living Rev. Relativity* **9**, 3 (2006).
- [2] D. Psaltis, *Living Rev. Relativity* **11**, 9 (2008).
- [3] C. M. Will, *Astrophys. J. Lett.* **674**, L25 (2008).
- [4] O. Dreyer, B. Kelly, B. Krishnan, L. S. Finn, D. Garrison, and R. Lopez-Aleman, *Classical Quantum Gravity* **21**, 787 (2004).
- [5] T. Johannsen and D. Psaltis, *Phys. Rev. D* **83**, 124015 (2011).
- [6] K. Glampedakis and S. Babak, *Classical Quantum Gravity* **23**, 4167 (2006).
- [7] A. N. Aliev and A. E. Gümrükçüoğlu, *Phys. Rev. D* **71**, 104027 (2005).
- [8] P. Pani, C. F. B. Macedo, L. C. B. Crispino, and V. Cardoso, *Phys. Rev. D* **84**, 087501 (2011).
- [9] M. Gilfanov and A. Merloni, *Space Sci. Rev.* **183**, 121 (2014).
- [10] R. A. Remillard and J. E. McClintock, *Annu. Rev. Astron. Astrophys.* **44**, 49 (2006).
- [11] A. C. Fabian, K. Iwasawa, C. S. Reynolds, and A. J. Young, *Publ. Astron. Soc. Pac.* **112**, 1145 (2000).
- [12] L. Brenneman, *Measuring the Angular Momentum of Supermassive Black Holes*, SpringerBriefs in Astronomy (Springer, New York, 2013).
- [13] C. S. Reynolds and M. A. Nowak, *Phys. Rep.* **377**, 389 (2003).
- [14] I. D. Novikov and K. S. Thorne, in *Black Holes (Les Astres Occlus)*, edited by C. Dewitt and B. S. Dewitt (Gordon and Breach, New York, 1973), p. 343.
- [15] J. E. McClintock, R. Narayan, S. W. Davis, L. Gou, A. Kulkarni, J. A. Orosz, R. F. Penna, R. A. Remillard, and J. F. Steiner, *Classical Quantum Gravity* **28**, 114009 (2011).
- [16] J. E. McClintock, R. Narayan, and J. F. Steiner, *Space Sci. Rev.* **183**, 295 (2014).
- [17] M. C. Weisskopf, R. Bellazzini, E. Costa, G. Matt, H. L. Marshall, S. L. O'Dell, G. G. Pavlov, B. Ramsey, and R. W. Romani, American Astronomical Society High Energy Astrophysics Division Annual Report, 2014, Vol. 14 (unpublished), p. 116.15.
- [18] K. Jahoda, C. Kouveliotou, T. R. Kallman, and Praxys Team, American Astronomical Society Meeting, Seattle, 2015, Abstract No. 225 (unpublished), p. 338.40.
- [19] P. Soffitta *et al.*, *Exp. Astron.* **36**, 523 (2013).
- [20] M. Beilicke *et al.*, *AIP Conf. Proc.* **1505**, 805 (2012).
- [21] M. Beilicke, F. Kislak, A. Zajczyk, Q. Guo, R. Endsley, M. Stork, R. Cowsik, P. Dowkontt, S. Barthelmy, T. Hams, T. Okajima, M. Sasaki, B. Zeiger, G. de Geronimo, M. G. Baring, and H. Krawczynski, *J. Astron. Instrum.* **03**, 1440008 (2014).
- [22] Q. Guo, M. Beilicke, A. Garson, F. Kislak, D. Fleming, and H. Krawczynski, *Astropart. Phys.* **41**, 63 (2013).
- [23] A. Ricarte and J. Dexter, *Mon. Not. R. Astron. Soc.* **446**, 1973 (2015).
- [24] L.-X. Li, R. Narayan, and J. E. McClintock, *Astrophys. J.* **691**, 847 (2009).
- [25] J. D. Schnittman and J. H. Krolik, *Astrophys. J.* **701**, 1175 (2009).
- [26] M. Dovčiak, F. Muleri, R. W. Goosmann, V. Karas, and G. Matt, *J. Phys. Conf. Ser.* **372**, 012056 (2012).
- [27] J. D. Schnittman and J. H. Krolik, *Astrophys. J.* **712**, 908 (2010).
- [28] E. Kara, A. Zoghbi, A. Marinucci, D. J. Walton, A. C. Fabian, G. Risaliti, S. E. Boggs, F. E. Christensen, F. Fuerst, C. J. Hailey, F. A. Harrison, G. Matt, M. L. Parker, C. S. Reynolds, D. Stern, and W. W. Zhang, *Mon. Not. R. Astron. Soc.* **446**, 737 (2015).
- [29] P. Uttley, E. M. Cackett, A. C. Fabian, E. Kara, and D. R. Wilkins, *Astron. Astrophys. Rev.* **22**, 72 (2014).
- [30] E. M. Cackett, A. Zoghbi, C. Reynolds, A. C. Fabian, E. Kara, P. Uttley, and D. R. Wilkins, *Mon. Not. R. Astron. Soc.* **438**, 2980 (2014).
- [31] D. R. Wilkins and A. C. Fabian, *Mon. Not. R. Astron. Soc.* **430**, 247 (2013).
- [32] C. Bambi and E. Barausse, *Astrophys. J.* **731**, 121 (2011).
- [33] C. Bambi, *Phys. Rev. D* **85**, 043002 (2012).
- [34] C. S. J. Pun, Z. Kovács, and T. Harko, *Phys. Rev. D* **78**, 084015 (2008).
- [35] C. Bambi, *Phys. Rev. D* **87**, 023007 (2013).
- [36] C. Bambi, *J. Cosmol. Astropart. Phys.* **08** (2013) 055.
- [37] T. Johannsen and D. Psaltis, *Astrophys. J.* **773**, 57 (2013).
- [38] D. Psaltis and T. Johannsen, *Astrophys. J.* **745**, 1 (2012).
- [39] H. Krawczynski, *Astrophys. J.* **754**, 133 (2012).
- [40] D. Liu, Z. Li, Y. Cheng, and C. Bambi, *Eur. Phys. J. C* **75**, 383 (2015).
- [41] T. Johannsen and D. Psaltis, *Astrophys. J.* **726**, 11 (2011).
- [42] C. Bambi, *J. Cosmol. Astropart. Phys.* **09** (2012) 014.
- [43] T. Johannsen, *Phys. Rev. D* **90**, 064002 (2014).
- [44] J. Jiang, C. Bambi, and J. F. Steiner, *J. Cosmol. Astropart. Phys.* **05** (2015) 025.
- [45] A. E. Broderick, T. Johannsen, A. Loeb, and D. Psaltis, *Astrophys. J.* **784**, 7 (2014).
- [46] C. Bambi, *Phys. Rev. D* **85**, 043001 (2012).
- [47] R. Narayan and J. E. McClintock, *Mon. Not. R. Astron. Soc.* **419**, L69 (2012).
- [48] T. Johannsen, *Phys. Rev. D* **87**, 124017 (2013).
- [49] N. I. Shakura and R. A. Sunyaev, *Astron. Astrophys.* **24**, 337 (1973).
- [50] D. N. Page and K. S. Thorne, *Astrophys. J.* **191**, 499 (1974).
- [51] S. Chandrasekhar, *Radiative Transfer* (Dover, New York, 1960).
- [52] G. Matt, G. C. Perola, and L. Piro, *Astron. Astrophys.* **247**, 25 (1991).
- [53] M. Dovciak, Ph. D. thesis, Charles University in Prague, 2004, <http://sirrah.troja.mff.cuni.cz/~dovciak/papers/thesis/phdthesis.pdf>.
- [54] I. M. George and A. C. Fabian, *Mon. Not. R. Astron. Soc.* **249**, 352 (1991).
- [55] L. Kong, Z. Li, and C. Bambi, *Astrophys. J.* **797**, 78 (2014).
- [56] L. Gou, J. E. McClintock, M. J. Reid, J. A. Orosz, J. F. Steiner, R. Narayan, J. Xiang, R. A. Remillard, K. A. Arnaud, and S. W. Davis, *Astrophys. J.* **742**, 85 (2011).
- [57] A. K. Kulkarni, R. F. Penna, R. V. Shcherbakov, J. F. Steiner, R. Narayan, A. Sądowski, Y. Zhu, J. E. McClintock, S. W. Davis, and J. C. McKinney, *Mon. Not. R. Astron. Soc.* **414**, 1183 (2011).
- [58] J. D. Schnittman and E. Bertschinger, *Astrophys. J.* **606**, 1098 (2004).
- [59] J. D. Schnittman, *Astrophys. J.* **621**, 940 (2005).
- [60] L. Stella and M. Vietri, *Astrophys. J. Lett.* **492**, L59 (1998).
- [61] L. Stella and M. Vietri, *Phys. Rev. Lett.* **82**, 17 (1999).

- [62] M. A. Abramowicz and W. Kluźniak, *Astron. Astrophys.* **374**, L19 (2001).
- [63] M. A. Abramowicz and W. Kluźniak, *Gen. Relativ. Gravit.* **35**, 69 (2003).
- [64] B. Beheshtipour, J. K. Hoormann, and H. Krawczynski (to be published).
- [65] P. Pihajoki, M. Valtonen, and S. Ciprini, *Mon. Not. R. Astron. Soc.* **434**, 3122 (2013).
- [66] T. E. Strohmayer, *Astrophys. J. Lett.* **552**, L49 (2001).
- [67] T. Johannsen and D. Psaltis, *Astrophys. J.* **718**, 446 (2010).
- [68] T. Johannsen, *Astrophys. J.* **777**, 170 (2013).
- [69] J. M. Bardeen, in *Black Holes (Les Astres Occlus)*, edited by C. Dewitt and B. S. Dewitt (Gordon and Breach, New York, 1973), p. 215.
- [70] C. Bambi, *Phys. Lett. B* **730**, 59 (2014).
- [71] K. S. Thorne, *Astrophys. J.* **191**, 507 (1974).
- [72] J. D. Schnittman and J. H. Krolik, *Astrophys. J.* **777**, 11 (2013).
- [73] J. D. Schnittman, J. H. Krolik, and S. C. Noble, *Astrophys. J.* **769**, 156 (2013).
- [74] A. Sądowski and R. Narayan, *Mon. Not. R. Astron. Soc.* **454**, 2372 (2015).